Phonons on II-VI (110) semiconductor surfaces

H. M. Tütüncü
Sakarya Üniversitesi, Fen-Edebiyat Fakültesi, Fizik Bölümü, Adapazarı, Turkey

R. Miotto and G. P. Srivastava
School of Physics, University of Exeter, Stocker Road, Exeter EX4 4QL, United Kingdom
(Received 16 November 1999; revised manuscript received 26 June 2000)

We have studied the phonon dispersion and density-of-states on the (110) surface of II-VI compounds CdTe, ZnTe, and ZnS in their zinc-blende phase by applying the adiabatic bond charge model. The relaxed surface atomic geometry and the corresponding bond charge information is obtained from the application of an *ab initio* pseudopotential calculation. The origins of various surface phonon modes are discussed and their variation for different compounds are analyzed in terms of the reduced mass and total mass differences. Furthermore, we have related some differences between surface modes on II-VI (110) and III-V (110) in terms of the ionicity factor.

I. INTRODUCTION

Microscopic investigations of atomic geometry, electronic states, and phonon modes on semiconductor surfaces are very important in view of their increasing role in electronic and optoelectronic devices. In general, most investigations have concentrated on atomic and electronic structure of surfaces of IV and III-V materials. In particular, studies of surface phonons have mostly been performed on the Si(001) and III-V (110) surfaces.[1,2] Relatively less attention has been paid towards investigations of surfaces of II-VI compounds. The atomic geometry of the (110) surface of zinc-blende II-VI compounds has been studied by low-energy electron diffraction (LEED)[3–6] and x-ray standing-wave measurements (XSW).[7] While angle-resolved photoemission (ARPE) experiments[8–12] have been used to map out the occupied surface electronic states of the ZnTe(110) and CdTe(110) surfaces, no such measurements are available for ZnS(110). On the theoretical side, atomic and electronic structures of II-VI (110) surfaces have been calculated using a tight-binding method[13,14] and a pseudopotential method within the local-density approximation.[15] However, no systematic efforts have been made to study phonon modes on II-VI (110) surfaces.

The adiabatic bond charge model, developed originally by Weber and co-workers for tetrahedrally bonded bulk materials,[16,17] has been extended to investigate phonons on surfaces of such materials.[18] Recently we have successfully employed the adiabatic bond charge model, in conjunction with atomic geometry and bonding results from *ab initio* pseudopotential method, to investigate phonon dispersion and density-of-states on III-V (110) surfaces.[19–21] The results obtained are in very good agreement with experimental measurements[22–24] as well as with *ab initio* calculations.[22,25,26] More recently, we have applied this procedure to study surface phonons on a ZnSe(110) surface.[27]

A thorough study of surface phonons on II-VI (110) is desirable. First of all, available results on III-V (110) surfaces will enable us to make comparison between surface phonons on III-V (110) surfaces and II-VI (110) surfaces. Although the bulk dispersion curves of these materials are similar to each other qualitatively, ionicity differences for these semiconductors produce quantitative differences in the phonon energies of II-VI compounds and III-V compounds.[28] For example InSb and CdTe have nearly the same bond length and average mass but the zone-center and zone-edge phonon frequencies for CdTe are lower than for InSb due to a higher ionicity factor. The larger ionicity of CdTe also causes a much larger LO-TO splitting at the Γ point and much larger LO-LA splitting at the X point (see Ref. 28). It can thus be expected that characteristics of surface phonons on II-VI (110) would be different from those on III-V (110).

In this paper we present a detailed and systematic study of surface phonons on ZnTe(110), CdTe(110), and ZnS(110) using the adiabatic bond charge model. The characteristic relaxed atomic geometry at these surfaces is determined by employing the *ab initio* pseudopotential method. The results of the pseudopotential calculations are also used to ascertain the bond charge along the dangling surface orbital.

II. METHOD

The main concept in the BCM is that the valence electron charge-density distribution in covalent bonded semiconductors is represented by massless bond charges (BC's), endowed with translational degrees of freedom. The interactions included in the BCM are the Coulomb interaction between all particles (ion-ion, ion-BC, and BC-BC), a central short-range interaction between nearest-neighbor particles, and a bond-bending interaction involving the BC-ion-BC angle.[16,17,28] This model produces bulk phonon dispersion curves for homopolar as well as heteropolar semiconductors, which are in very good agreement with experimental neutron-scattering data[29–32] and *ab initio* phonon calculations.[33,34]

In general a BC is placed at the maximum of the electronic charge density along a bond. Thus BC's in homopolar semiconductors (such as Ge and Si) are positioned in the middle of bond lengths, while in III-V semiconductors they

are displaced towards anions, dividing a bond in the ratio 3:5. On the other hand, the maxima of electronic charge density along the tetrahedral bonds in II-VI semiconductors do not divide the bond lengths in the ratio 2:6 but in the ratio close to 1:2.[35] We also observed this ratio for the II-VI compounds in our *ab initio* pseudopotential calculations, as described below. If r_0 indicates the bond length and $r_1=(1+p)r_0/2$ and $r_2=(1-p)r_0/2$ indicate the cation-BC and anion-BC distances respectively, then the parameter p takes the values 0, 1/4, and 1/3 for IV, III-V, and II-VI semiconductors, respectively.

For surface phonon calculations we have modeled the II-VI (110) surface in a repeated slab scheme. The supercell consisted of 11 layers of II-VI, and a vacuum region equivalent to eight atomic layers. The atoms in the top three layers on each side were placed at their relaxed positions while deeper lying atoms were taken in their bulk positions. Bond charges were, in general, placed along the bonds between two ions using the p factor described earlier. However, the BC's representing the surface dangling bonds were placed according to the maximum valence electron density obtained from the pseudopotential calculations (see Results section).

In order to apply the BCM to the II-VI (110) surfaces, the interactions described above are used. However, as the ionic environments in the bulk and at the surface are different, the force constants for bulk and surface geometries will also be different. For the surface calculations we have scaled the second derivatives of the central ion-ion and ion-BC potentials (ϕ'') as

$$\phi''_{\text{surface}}=\frac{r^2_{\text{bulk}}}{r^2_{\text{surface}}}\phi''_{\text{bulk}}, \tag{2.1}$$

where r_{bulk} and r_{surface} denote the magnitude of the relative distance between particles (ion-ion, ion-BC, and BC-BC) for bulk and surface, respectively. The validity of this assumption has been established in tight-binding electronic structure calculations.[36,37] The bond-bending potential used in bulk BCM calculations is given as

$$V^{(\sigma)}_{bb}=\frac{1}{2}B_\sigma(\mathbf{r}_{\sigma i}\cdot\mathbf{r}_{\sigma j}+a^2_\sigma)^2/4a^2_\sigma, \tag{2.2}$$

where $\mathbf{r}_{\sigma k}$ is the distance vector between the ion type σ and its neighboring bond charge k, a^2_σ is the equilibrium value of $|\mathbf{r}_{\sigma i}\cdot\mathbf{r}_{\sigma j}|$, and B_σ is the bond-bending force constant. The bulk values of the bond-bending force constant parameters B_1 and B_2 were also used for surface calculations. However, it should be appreciated that the elements of the short-range bond-bending ion-BC matrices between the top layer atoms and their neighboring BC's will become very different from their bulk values because the dot product $\mathbf{r}_{\sigma i}\cdot\mathbf{r}_{\sigma j}$ for neighboring BC's will change considerably for the relaxed geometries of surfaces.

In order to calculate the relaxed atomic geometry we modeled the II-VI (110) surface in a repeated slab scheme and employed a self-consistent pseudopotential method within the local-density approximation.[2] We considered an atomic slab with seven layers of II-VI substrates and a vacuum region equivalent of six substrate atomic layers. The electron-ion interaction was considered in the form of *ab initio* norm conserving pseudopotentials.[38] The electron-electron exchange-correlation interaction was considered within the local-density approximation.[39] The $3d$ electrons in Zn and the $4d$ electrons in Cd were treated as core electrons but their influence on valence states was taken into account by applying the nonlinear core correction.[40] The calculated bulk lattice constant values of 6.43 Å, 6.08 Å, and 5.35 Å for CdTe, ZnTe, and ZnS, respectively, were used for surface atomic geometry optimization as well as for surface phonon calculations. Self-consistent solutions to the Kohn-Sham equations were obtained by employing a set of four special **k** points within the irreducible part of the surface Brillouin zone.[2] Well converged atomic geometry and electronic structure results were obtained by considering a basis of plane waves up to the kinetic-energy cutoff of 16 Ry.

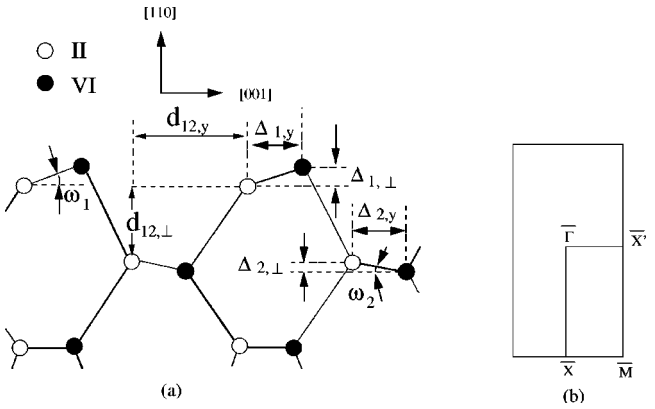

FIG. 1. (a) Schematic relaxed side view of II-V (110) surface. (b) The corresponding surface Brillouin zone.

III. RESULTS

A. Atomic geometry and electronic structure

Before discussing our results for surface phonons, we will discuss the results for atomic geometry and electronic structure. The calculated surface structural parameters, indicated in Fig. 1, are shown in Table I. A comparison of our results with previous experimental and theoretical results is also presented. As seen in Fig. 1, the II-VI (110) surfaces show a well-established relaxation pattern. At the surface layer the anion moves away from the bulk in favor of an s^2p^3 bonding with three neighboring cations, resulting in a pyramidal geometry. The cation on the surface moves into the bulk in favor of an sp^2 bonding with three neighboring anions resulting in a planar geometry. The relative displacement of the cation and the anion defines a tilt angle, ω_1, which characterizes the extent of surface relaxation. The tilt angles for ZnTe(110), CdTe(110), and ZnS(110) surfaces are found to be 29.6°, 30.4°, and 27.1°, respectively. The vertical buckling of the top layer, $\Delta_{1,\perp}$, is 0.195 Å, 0.199 Å, and 0.191 Å for ZnTe(110), CdTe(110), and ZnS(110), respectively. The presently calculated values of the key surface structural parameters ω_1, $\Delta_{1,\perp}$, $d_{12,\perp}$, and $\Delta_{1,y}$ are in good agreement with the results obtained from LEED studies,[4,3,6] XSW studies,[7] and previous theoretical calculations.[7,14,15]

The electronic band structures for ZnTe(110), CdTe(110), and ZnS(110) are shown in Fig. 2. Our results compare well with the available angle-resolved photoemission results[8,11,12]

TABLE I. Atomic geometry of the ZnTe(110), CdTe(110), and ZnS(110) surfaces. The presently calculated results are compared with other theoretical and experimental data. All of the distance are given in terms of the bulk lattice constant (a_0) while the angles are in degrees.

	a_0 (Å)	$d_{12,\perp}$	$d_{12,y}$	$\Delta_{1,\perp}$	$\Delta_{1,y}$	$\Delta_{2,\perp}$	$\Delta_{2,y}$	ω_1	ω_2
					ZnTe(110)				
Present	6.08	0.248	0.426	0.111	0.195	0.017	0.248	29.6	−4.0
LEED (Ref. 4)								28	
					CdTe(110)				
Present	6.43	0.252	0.422	0.117	0.199	0.023	0.253	30.4	−5.2
LEED (Ref. 3)		0.241	0.594	0.127	0.215	0.028		30.5	
LEED (Ref. 6)		0.245	0.560	0.127	0.215	0.013		30.5	
TB (Ref. 14)		0.247	0.580	0.117	0.208	0.039		29.3	
XSW (Ref. 7)				0.120	0.219			28.7	
LDA (Ref. 7)		0.255	0.573	0.114	0.201	0.020		29.5	
					ZnS(110)				
Present	5.35	0.254	0.435	0.098	0.191	0.017	0.248	27.1	−4.1
LEED (Ref. 4)								25	
TB (Ref. 13)		0.259	0.566	0.114	0.221			27.40	

for ZnTe(110) and CdTe(110). In general, the number of surface states on these II-VI (110) surfaces, and their energy locations, are very similar to that obtained for III-V (110) surfaces,[41] and thus will not be discussed in detail. However, it will be useful for surface phonon calculations to point out that for the relaxed atomic geometry the dangling bonds of the surface cations result in an empty band near the bulk conduction-band minimum and that the dangling bonds of the anions give rise to a rather dispersionless filled band near the bulk valence-band maximum. Figure 2 also presents the location of the anion dangling BC for all the surfaces considered in this paper.

B. Phonon-dispersion curve and density-of-states

The force constants used for the adibatic bond charge calculations of the bulk phonon spectra for CdTe, ZnTe, and ZnS are taken from Ref. 28. These are then modified for the surface calculations according to Eq. (2.1). The calculated surface phonon dispersion curves and the density-of-states for CdTe(110), ZnTe(110), and ZnS(110) are shown in Fig. 3. Also shown in that figure are the bulk spectra projected on the (110) surface (hatched regions) and the bulk density-of-states (dashed curve). We first briefly discuss the bulk phonon characteristics. We find that there is a trend in the bulk phonon spectrum of the compounds studied here: the acoustic and optical band-edge frequencies, as well as the acoustic-optical band gap, increase as we move along CdTe, ZnSe, and ZnS. In addition, we find that ZnS is characterized by two almost equal intensity peaks in the density-of-states in the optical range.

The calculated surface phonon modes are in general either localized modes or resonant modes. Surface localized modes are in general found below the acoustic spectrum at the zone edges (known as Rayleigh modes[42]) in stomach gaps within the projected bulk acoustic spectrum, within the band gaps, and above the optical spectrum (known as the Fuchs-Kliewer mode[43]). The Rayleigh modes, which arise from reduced atomic coordination at the surface, are found to lie slightly below the acoustic spectrum for ZnTe(110) and ZnS(110). There are three localized modes lying in the acoustic stomach gap for CdTe(110), while for ZnTe(110) and ZnS(110) there are only two such modes. For ZnS(110) we obtained a total of four surface phonon branches in the large acoustic-optical bulk band gap, three of which are truely localized through the surface Brillouin zone. These modes give rise to a clear peak in the density-of-states between the bulk acoustic and optical-phonon regions for ZnS. For CdTe(110) and ZnTe(110) we have found only one surface state, leading to a rather small peak in the density-of-states within the acoustic-optical gap region. For all the three surfaces we found the highest surface optical mode (the so-called Fuchs-Kliewer mode) to be truly localized for wave vectors along the directions $\bar{X}$-$\bar{M}$ and $\bar{M}$-$\bar{X}'$.

C. Characteristics of surface phonons

In this section we analyze the polarization characteristics of phonons on these surfaces. To facilitate the discussion we will present the results at the zone center in some detail and analyze changes as the wave vector moves away from the zone center. It is useful to note that the cation/anion mass ratio is 0.88, 0.51, and 2.04 for CdTe, ZnTe, and ZnS, respecively.

1. Zone center phonons

At the zone center we have identified four interesting types of surface modes on II-VI (110), similar to those seen on III-V (110) surfaces.[19] These are rotational, bond stretching, gap, and Fuchs-Kliewer phonon modes.

The lowest optical surface modes at the zone center are calculated at 5.90, 7.71, and 12.34 meV for CdTe(110), ZnTe(110), and ZnS(110), respectively. These results compare well with the rotational mode at 4.8 and 13.7 meV calculated by Wang and Duke[44] for CdTe(110) and ZnS(110), respectively. Although these modes involve vibrations of atoms up to four atomic layers, as shown in Fig. 4, the most significant contribution comes from the top layer atoms in the form of rotation of the cation-anion bond. For

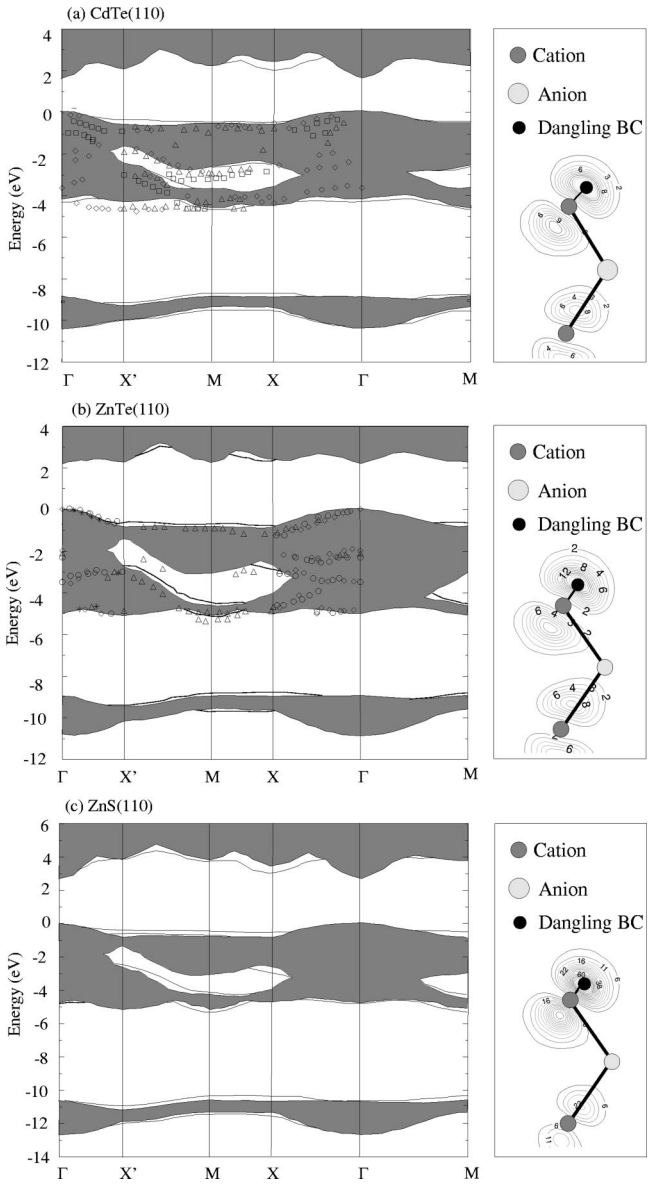

FIG. 2. The electronic band structure and electronic charge density for the highest occupied dangling bond states of the II-VI (110) surface. The projected bulk spectrum is shown by hatched regions. The calculated localized electronic states are shown by solid curves. The ARPE data for CdTe(110) are shown as open squares (Ref. 8), and as open triangles and open diamonds (Ref. 12). The ARPE data for ZnTe(110) (Ref. 11) are shown as open diamonds (23 eV photon energy), open circles (25 eV), and open triangles (31 eV).

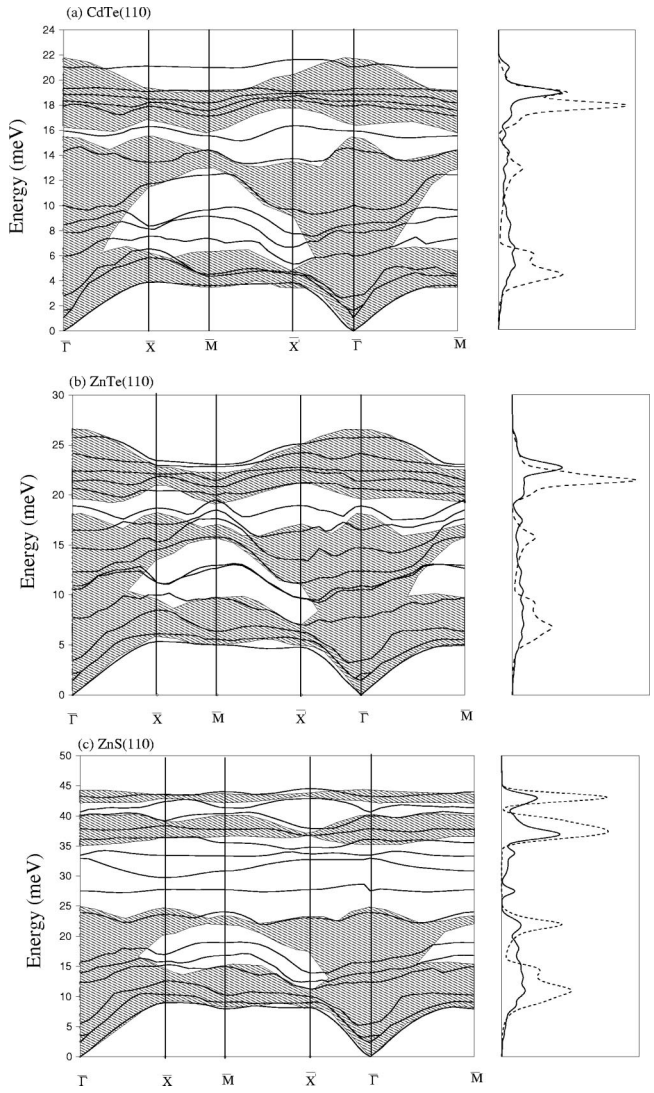

FIG. 3. Phonon-dispersion curves and density of phonon states of the II-VI (110) surfaces. For phonon-dispersion curves, the calculated results are shown by thick-solid curves while bulk projection is shown by hatched region. For the density of phonon states, the solid curve is obtained from the (110) slab supercell calculation with the relaxed surface geometry, while the dotted curve shows the bulk density-of-states.

all the surfaces considered we have identified a bond-stretching phonon mode that lies at 14.30, 16.50, and 23.43 meV for CdTe(110), ZnTe(110), and ZnS(110), respectively. This mode (see Fig. 5) results mainly from roughly equal magnitudes of cationic and anionic vibrations at the top layer on CdTe(110) and ZnTe(110), but also shows significant cationic vibrations in the second and third layers for ZnS(110).

The acoustic-optical gap is the smallest for CdTe and the largest for ZnS, in accordance with their cation-anion mass differences. We have calculated one gap localized mode for CdTe(110) and ZnTe(110), and three such modes for ZnS(110). The atomic vibrational pattern for the three truly localized modes on ZnS(110) are shown in Fig. 6. The mode with the lowest energy can be interpreted as a bond stretching mode in the top two surface layers. It is interesting to note that this mode has a similar bond-stretching behavior to that found at 23.43 meV (cf. Fig. 5), except that at this energy it is the anion (with smaller mass than cation) which has a much larger atomic vibrational amplitude. The second gap mode is totally polarized along the cation-anion chain in the top surface layer, i.e., has the A'' representation.[19] The third gap mode is also an anionic vibrational mode, charaterized by the opposing motion of the first- and second-layer S atoms along the surface normal direction. The zone-center gap modes at 15.94 meV and 18.91 meV in the acoustic-optical gap of CdTe and ZnTe, respectively, have the A' representation, i.e., are polarized in a plane normal to the chain direction.

The frequency of the Fuchs-Kliewer surface phonon mode can be calculated[45] from the expression

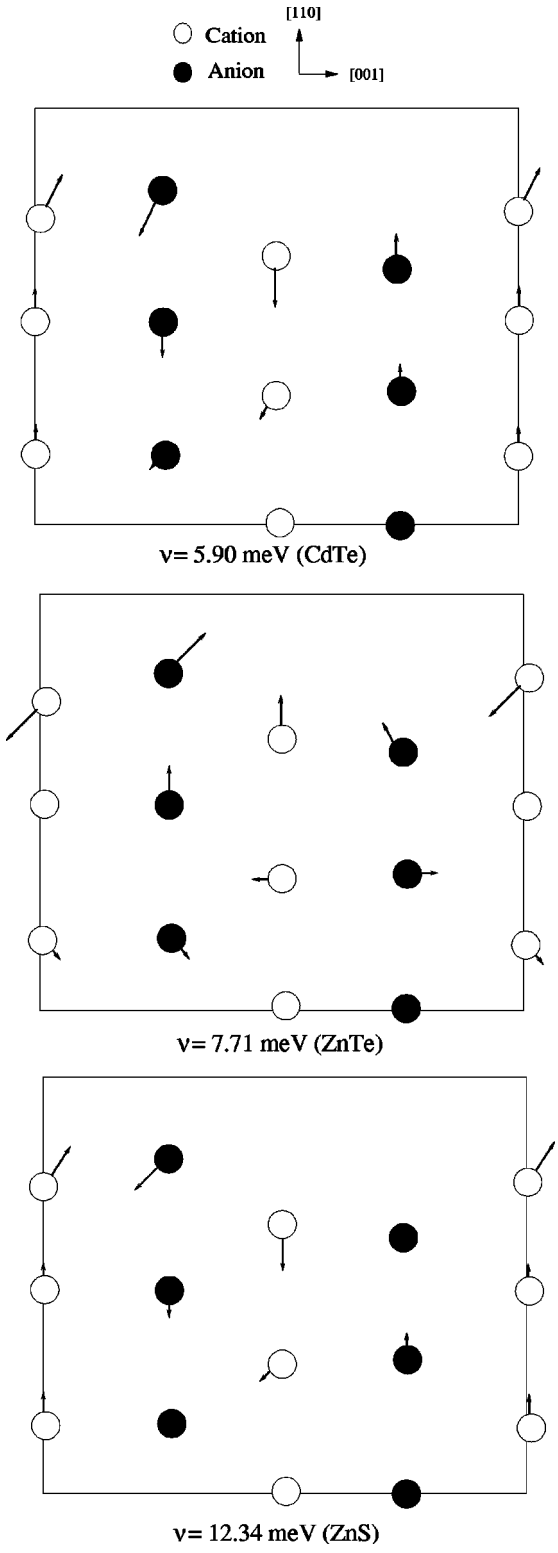

FIG. 4. Atomic displacement patterns for the rotational phonon mode on the ZnTe(110), CdTe(110), and ZnS(110) surfaces at the $\bar{\Gamma}$ point.

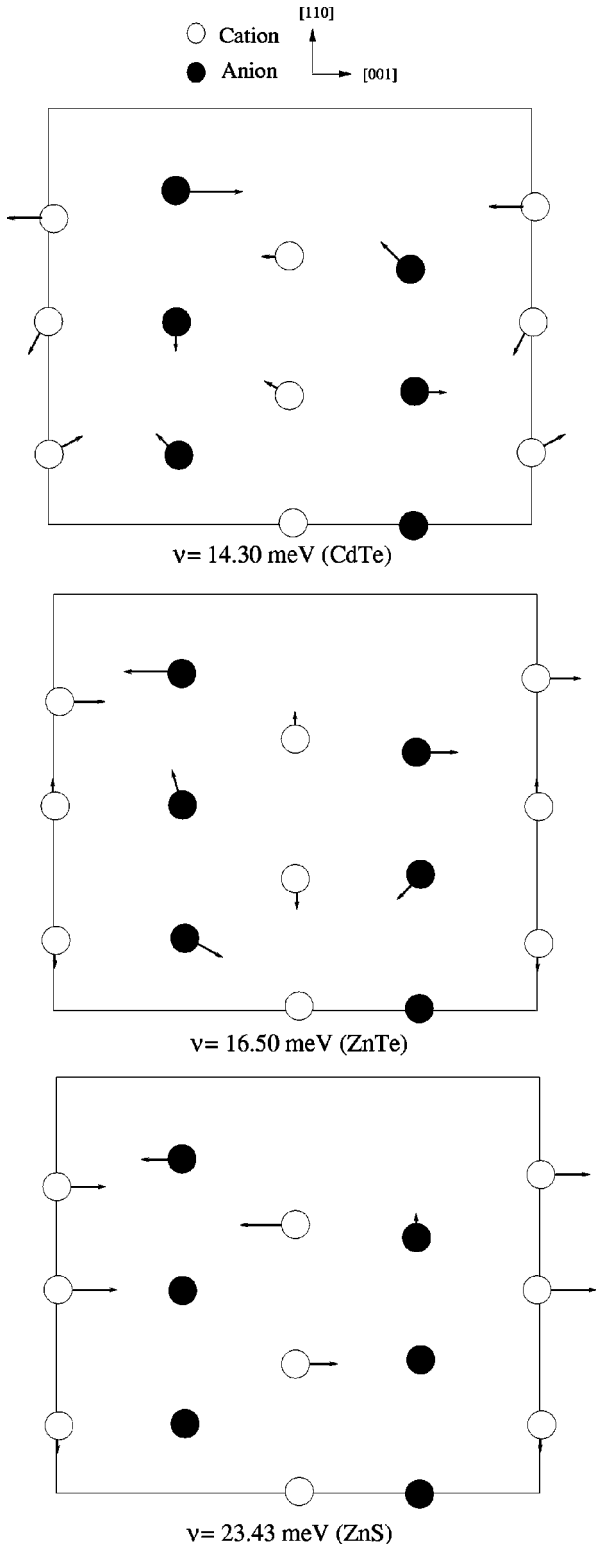

FIG. 5. Atomic displacement patterns for the bond-stretching phonon mode on the ZnTe(110), CdTe(110), and ZnS(110) surfaces at the $\bar{\Gamma}$ point.

$$\omega_{FK}=\omega_{\mathrm{TO}}[(\varepsilon_0+1)/(\varepsilon_\infty+1)]^{1/2}. \tag{3.1}$$

Accordingly, using experimental values for ω_{TO}, ε_0, and ε_∞,[45,46] this mode should occur at 22.0, 25.0, and 42.0 meV for CdTe(110), ZnTe(110), and ZnS(110), respectively. From our work, we have calculated this mode at 21.05, 25.80, and 43.25 meV for CdTe(110), ZnTe(110), and ZnS(110), respectively, lending strong support to the validity of Eq. (3.1). For all the three surfaces this mode originates from the vibrations of the second- and third-layer atoms, as shown in Fig. 7. However, there is a difference in the details of the atomic displacement pattern at these surfaces. For

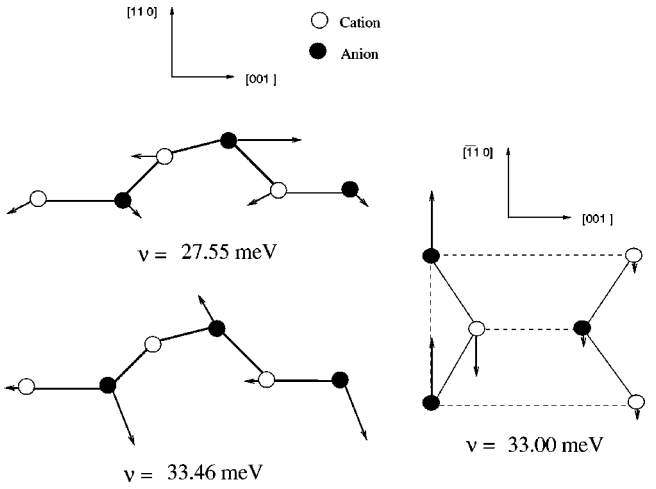

FIG. 6. Atomic displacement patterns of gap phonon modes on the ZnS(110) surface at the $\overline{\Gamma}$ point.

CdTe(110) and ZnTe(110) the cation and anion in each of the second and third layers vibrate against each other. This behavior is similar to that observed on the InSb(110) surface[20,48] for which the cation and anion masses are nearly equal. The vibrational pattern for ZnS(110) is very different: the anion vibrate with very large amplitude due to their much smaller mass. Similar behavior has been found for GaP(110) and InP(110), where anionic mass is much smaller than the cationic mass.[19,47]

2. Phonon modes away from the zone center

Surface phonon modes in general show some dispersion as the surface wave vector increases from the zone center towards a zone boundary. However, the modes that are localized at the zone center tend to remain so throughout the zone. In addition, some of the modes that are resonant at the zone center, turn into localized modes in different parts of the zone. In particular, along the directions $\overline{\Gamma}$-$\overline{M}$, $\overline{X}$-$\overline{M}$, and $\overline{M}$-$\overline{X'}$ localized modes develop in the ''stomach'' gap within the acoustic region. At the zone edges there is a clear development of the Rayleigh mode below the acoustic continuum. Also, the Fuchs-Kliewer mode becomes a localized mode, with frequency above the bulk optical continuum, along the directions $\overline{\Gamma}$-$\overline{M}$, $\overline{X}$-$\overline{M}$, and $\overline{M}$-$\overline{X'}$.

We have identified up to three surface acoustic phonon modes at the zone edges $\overline{X}$ and $\overline{X'}$. The frequencies of these modes lie close to the lower end of the bulk acoustic continuum. For CdTe(110) at $\overline{X'}$ their frequencies are 3.84, 4.52, and 4.79 meV, and the corresponding vibrational patterns are polarized as A', A'', and A', respectively. The A' modes are contributed by the higher-lying transverse acoustic (T_1A) and longitudinal acoustic (LA) bulk modes and the A'' mode is derived from the lower-lying transverse acoustic bulk T_2A modes. For ZnTe(110) we have identified only two such modes, at 4.76 meV with polarization A' and at 5.51 meV with polarization A''. For ZnS(110) we could only identify the lowest mode at 8.18 meV with the A' polarization. Clearly, thus, the lowest-lying surface acoustic mode on all these surfaces, i.e., the Rayleigh mode, is of the A' character. The mixed $T_1A\otimes$ LA character of the Rayleigh mode at $\overline{X'}$

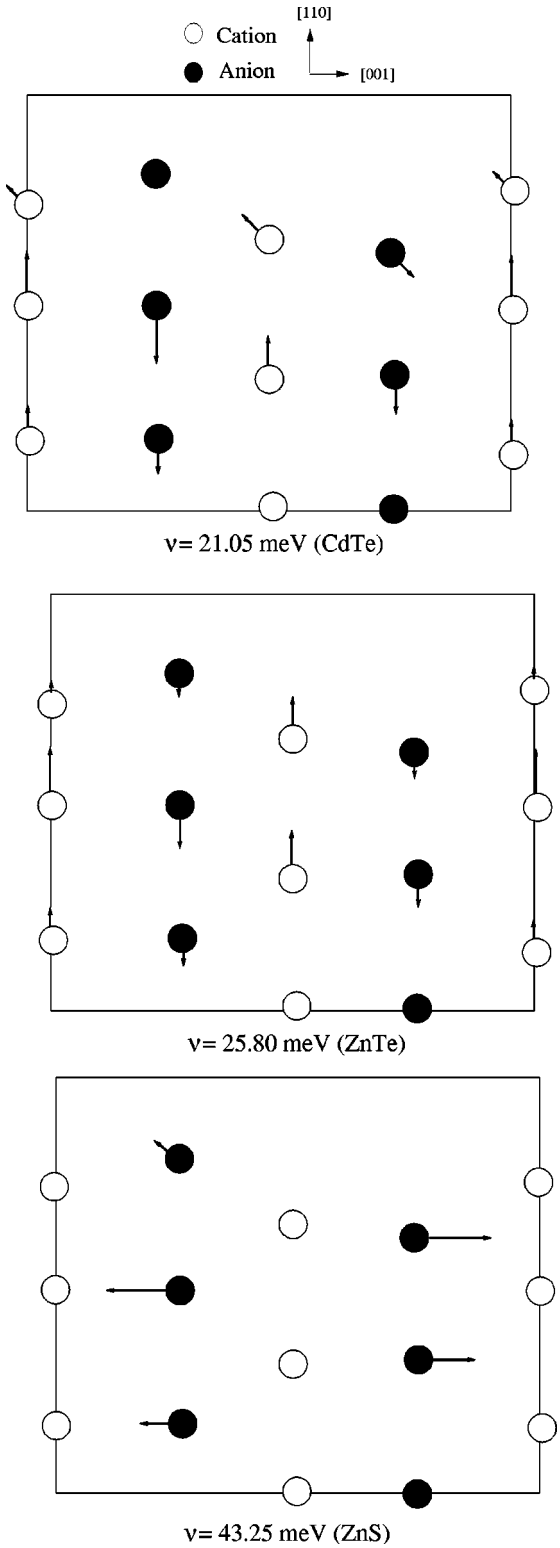

FIG. 7. Atomic displacement patterns of the Fuchs-Kliewer phonon mode on the ZnTe(110), CdTe(110), and ZnS(110) surfaces at the $\overline{\Gamma}$ point.

is also observed at the $\overline{X}$ point. However, we find that the Rayleigh mode at a given symmetry point on the zone can be contributed by the surface anions and cations vibrating in different directions. For example, at $\overline{X'}$ we find that for CdTe(110) the displacement pattern of this mode consists of the top layer and the second-layer anion atoms vibrating

along the surface normal direction. In contrast, for the same mode on ZnS(110) the roles of cation and anion are exchanged.

The lowest-energy acoustic-optical gap mode on ZnS(110), with a bond-stretching character, is nearly flat along the surface Brillouin zone. The third gap phonon mode on ZnS(110) originates from vibrations mainly of the first- and second-layer anions and shows little dispersion throught the zone. The second gap mode, with energy 33.00 meV and polarization A'' at the zone center, shows appreciable dispersion along the $\bar{\Gamma}$-$\bar{X}$ and $\bar{M}$-$\bar{X}$ directions. However, it is almost dispersionless along $\bar{\Gamma}$-$\bar{X'}$, indicating that the interaction between the vibrations of neighboring chains on the surface is negligible. This is a characteristic feature of the A'' gap phonon mode seen on many III-V (110) surfaces.[19]

D. Similarities and mass trends

Our paper shows that surface phonons on II-VI (110) have many similarities with their counterparts on III-V (110). In addition, we find that, as observed for III-V (110), there are predictable mass trends for some of the phonon modes on II-VI (110). The original observation by Wang and Duke[44] of a zone-center rotational phonon mode on III-V (110) and II-VI (110) has been verified in several other works, including this one. This phonon mode is a surface optical-phonon mode with opposing motions of first-layer atoms in the surface normal direction. Figure 8(a) shows the variation of the frequency of this phonon mode on a few II-VI (110) surfaces against the square root of the inverse reduced mass of the cation and anion. The results suggest that the energy of this phonon mode for different II-VI (110) surfaces has a clear linear dependence on the reduced mass. As seen in Fig. 8(a), the frequencies of the rotational mode, bond-stretching mode and the Fuchs-Kliewer phonon mode also show a linear variation with the reduced mass. The frequency of the Rayleigh mode shows a linear variation with the inverse square root of the total mass (i.e., sum of the cation and anion masses), as it can be seen in Fig. 8(b). Such a variation is expected as the Rayleigh mode is a surface acoustic mode.

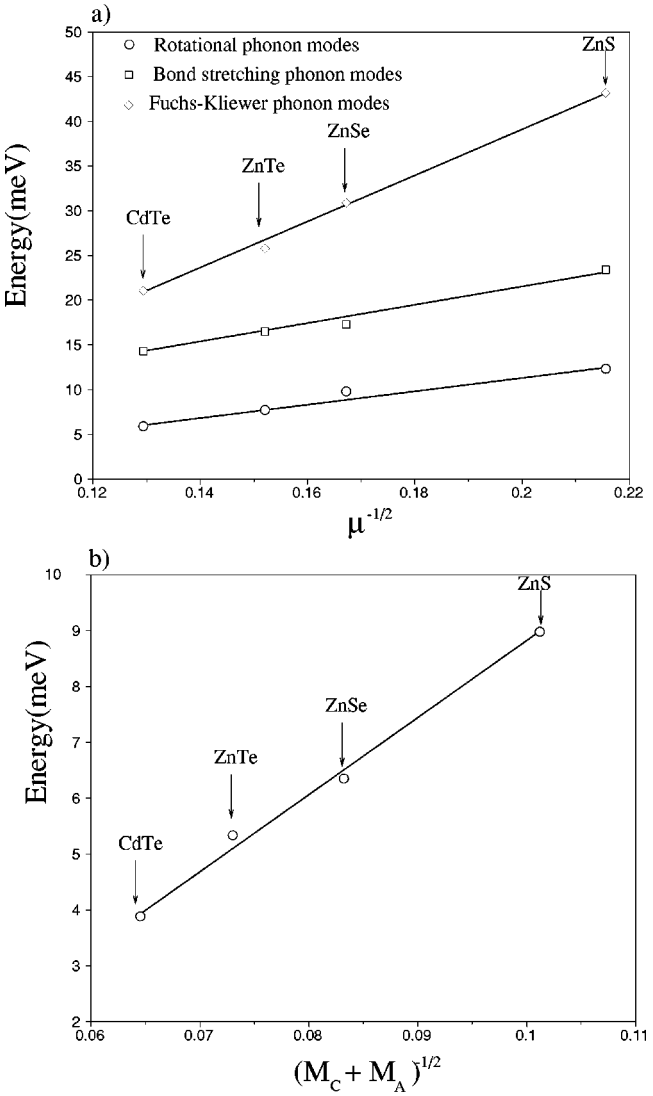

FIG. 8. (a) The rotational, bond-stretching and Fuchs-Kliewer frequencies of II-VI (110) surfaces at the $\bar{\Gamma}$ point against the square root of the reduced mass (μ) of the cation and anion. (b) The Rayleigh mode on II-VI (110) surfaces at the $\bar{X}$ point against the square root of inverse total mass of surface cation and anion.

E. Comparison of surface phonons on the CdTe(110) and InSb(1110)

It is interesting to compare the phonon modes on the CdTe(110) and InSb(110) surfaces. While CdTe and InSb have similar lattice constant and similar total as well as reduced mass per unit primitive cell, CdTe is much more ionic than InSb. This, in general, has the effect of lowering the phonon frequencies, and producing a larger LO-TO splitting at the Γ point and a much larger LO-LA splitting at the X point in CdTe when compared to InSb.[28] The characteristics of surface phonon modes on CdTe(110) and InSb(110) surfaces reflect the differences mentioned above. We have noted, for example, that there is a finite amount of acoustic-optical gap in CdTe, due to larger LO-LA splitting, allowing the development of localized gap surface modes in this range.

Table II lists a comparison of the calculated[48] surface phonon modes on CdTe(110) and InSb(110) according to their energy locations and the A', A'' polarization characters at the $\bar{\Gamma}$ and $\bar{X'}$ points. All the modes listed in the table have similar displacement pattern for the two surfaces, and since the average and reduced masses are similar, the differences in their energies can be explained on the basis of the ionicity difference. As the surface acoustic modes are not affected by ionicity, such modes are found to lie at similar energies for the two surfaces (cf. columns 1 and 3 at the $\bar{X'}$ point in Table II). In general, the surface optical modes on CdTe(110) are found at lower energies than their counterparts on InSb(110). In addition, the presence of one localized phonon mode in the acoustic-optical gap region for CdTe(110) can be ascribed to the larger ionicity of this material. In contrast, no such localized modes are observed on InSb(110).[20]

IV. SUMMARY

We have presented the results of adiabatic bond-charge calculations for surface phonons on the (110) surface of

TABLE II. Calculated surface phonon frequencies (in meV) for InSb(110) and CdTe(110) at the $\overline{\Gamma}$ and $\overline{X'}$ points. RM, BS, and FK indicate the rotational mode, bond-stretching mode and the Fuchs-Kliewer frequency, respectively.

Mode	A''		A'			
		At the $\overline{\Gamma}$ point				
InSb(110) (Refs. 48,20)	19.95	21.98	6.92	15.62	20.94	24.03
CdTe(110)	17.93	18.84	5.90	14.30	18.35	21.05
			RM	BS		FK
		At the $\overline{X'}$ point				
InSb(110) (Refs. 48,20)	4.05	19.95	3.92	16.51	20.25	23.69
CdTe(110)	4.52	17.99	3.84	13.74	18.38	21.63

CdTe, ZnTe, and ZnS. In order to make such calculations we have inputted the relaxed atomic geometry and electronic structure of these surfaces, which in turn have been obtained from first-principles total-energy calculations. The presently calculated surface atomic geometry is in good agreement with the results obtained from LEED studies and from previous theoretical calculations. Similarly, our calculated surface electronic structures for CdTe(110) and ZnTe(110) are in good agreement with angle-resolved photoemission measurements.

In general, the surface phonon modes follow certain mass trends: the energy of surface acoustic Rayleigh mode varies linearly with the inverse square root of the sum of the cation and anion masses, and the energy of surface optical modes (such as the rotational, bond-stretch, gap, and Fuchs-Kliewer modes) varies linearly with the inverse square root of the reduced mass. However, the polarization characteristics of some surface optical modes on ZnS(110) are different from their counterparts for CdTe(110) and ZnTe(110). This is largely due to the much larger cation-anion mass difference for ZnS than for the other two materials. The influence of the mass difference between Zn and S is reflected in the fact that the highest surface optical mode on ZnS(110) is exclusively an anionic mode. Finally, it has been pointed out that the difference in the surface lattice dynamics on the (110) surface of the isoelectronic materials CdTe and InSb is due to these being characterized by different levels of ionicity.

ACKNOWLEDGMENTS

This work was supported by the Scientific and Technical Research Council of Turkey (TUBITAK). R. Miotto acknowledges financial support from Fundação de Amparo à Pesquisa do Estado de São Paulo (FAPESP), Brazil.

[1] See, e.g., G.P. Srivastava, Rep. Prog. Phys. **60**, 561 (1997) and references therein.
[2] G.P. Srivastava, *Theoretical Modeling of Semiconductor Surfaces* (World Scientific, Singapore, 1999).
[3] C.B. Duke, A. Paton, W.K. Ford, A. Kahn, and G. Scott, Phys. Rev. B **24**, 3310 (1981).
[4] A. Kahn, Surf. Sci. Rep. **3**, 193 (1983).
[5] C.B. Duke, in *Surface Properties of Electronic Materials*, edited by D.A. King and D.P. Woodruff (Elsevier, Amsterdam, 1987), Chap. 3.
[6] C. Cowell and V.E. de Carvalho, J. Phys. C **21**, 2983 (1988).
[7] T. Kendelewicz, J.E. Klepeis, J.C. Woicik, S.H. Southworth, C. Mailhiot, M. van Schilfgaarde, M. Methfessel, A. Herrera-Gomez, and K.E. Miyano, Phys. Rev. B **51**, 10 774 (1995).
[8] K.O. Magnusson, S.A. Flodström, and P.E.S. Persson, Phys. Rev. B **38**, 5384 (1988).
[9] B.A. Orlowski, J.P. Lacharme, S. Bensalah, and C.A. Sebenne, Surf. Sci. Lett. **200**, 460 (1988).
[10] H. Qu, P.O. Nilsson, J. Kanski, and L. Ilver, Phys. Rev. B **39**, 5276 (1989).
[11] H. Qu, J. Kanski, P.O. Nilsson, and U.O. Karlsson, Phys. Rev. B **43**, 9843 (1991).
[12] H. Qu, J. Kanski, P.O. Nilsson, and U.O. Karlsson, Phys. Rev. B **43**, 14 589 (1991).
[13] Y.R. Wang and C.B. Duke, Phys. Rev. B **36**, 2763 (1987).
[14] Y.R. Wang, C.B. Duke, K.O. Magnusson, and S.A. Flodström, Surf. Sci. **205**, L760 (1988).
[15] D. Vogel, P. Krüger, and J. Pollmann, Surf. Sci. **402-404**, 774 (1998).
[16] W. Weber, Phys. Rev. Lett. **33**, 371 (1974).
[17] K.C. Rustagi and W. Weber, Solid State Commun. **18**, 673 (1979).
[18] P. Santini, L. Miglio, G. Benedek, U. Harten, P. Ruggerone, and J.P. Toennies, Phys. Rev. B **42**, 11 942 (1990).
[19] H.M. Tütüncü and G.P. Srivastava, J. Phys. Chem. Solids **58**, 685 (1997).
[20] H.M. Tütüncü, M. Çakmak, and G.P. Srivastava, Appl. Surf. Sci. **123**, 146 (1998).
[21] H.M. Tütüncü and G.P. Srivastava, Phys. Rev. B **59**, 4925 (1999).
[22] M.B. Nardelli, D. Cvetko, V. De Renzi, L. Floreano, A. Morgante, M. Peloi, and F. Tommasini, Phys. Rev. B **52**, 16 720 (1995).
[23] H. Nienhaus and W. Mönch, Surf. Sci. **328**, L561 (1995).
[24] H. Nienhaus, Phys. Rev. B **56**, 13 194 (1997).
[25] J. Fritsch, P. Pavone, and U. Schröder, Phys. Rev. Lett. **71**, 4194 (1993).
[26] J. Fritsch, P. Pavone, and U. Schröder, Phys. Rev. B **52**, 11 326 (1995).

[27] H.M. Tütüncü and G.P. Srivastava, Phys. Rev. B **57**, 3791 (1998).
[28] B.D. Rajput and D.A. Browne, Phys. Rev. B **53**, 9052 (1996).
[29] G. Nilsson and G. Nelin, Phys. Rev. B **3**, 364 (1971).
[30] D.L. Price, J.M. Rowe, and R.M. Nicklow, Phys. Rev. B **3**, 1268 (1971).
[31] J.M. Rowe, R.M. Nicklow, D.L. Price, and K. Zanio, Phys. Rev. B **10**, 67 (1974).
[32] N. Vagelatos, D. Wehe, and J.S. King J. Chem. Phys. **60**, 3613 (1974).
[33] P. Giannozzi, S. De Gironcoli, P. Pavone, and S. Baroni, Phys. Rev. B **43**, 7231 (1991).
[34] A.D. Corso, S. Baroni, and R. Resta, Phys. Rev. B **47**, 3588 (1993).
[35] J.R. Chelikowaski and M.L. Cohen, Phys. Rev. B **14**, 556 (1976).
[36] D.C. Allan and E.J. Mele, Phys. Rev. Lett. **53**, 826 (1984).
[37] A. Mazur and J. Pollmann, Phys. Rev. Lett. **57**, 1811 (1986).
[38] N. Troullier and J.L. Martins, Phys. Rev. B **43**, 1992 (1991).
[39] D.M. Ceperley and B.I. Alder, Phys. Rev. Lett. **45**, 566 (1980).
[40] S.G. Louie, S. Froyen, and M.L. Cohen, Phys. Rev. B **26**, 17 382 (1982).
[41] A. Umerski and G.P. Srivastava, Phys. Rev. B **51**, 2334 (1995).
[42] Lord Rayleigh, Proc. London Math. Soc. **17**, 4 (1887).
[43] R. Fuchs and K.L. Kliewer, Phys. Rev. **140**, 2076 (1965).
[44] Y.R. Wang and C.B. Duke, Surf. Sci. **205**, L755 (1988).
[45] W. Mönch, *Semiconductor Surfaces and Interfaces* (Springer-Verlag, Berlin, 1995).
[46] Landolt-Börnstein, *Numerical Data and Functional Relationships in Science and Technology* (Springer-Verlag, Berlin, 1982).
[47] H.M. Tütüncü, Ph.D. thesis, University of Exeter, U.K., 1998.
[48] Note that our theoretical lattice constant for InSb, 6.30 Å, is slightly smaller than our theoretical lattice constant, 6.43 Å, for CdTe. This difference should not alter our conclusion.